

Influence of Embedded Nanocontainers on the Efficiency of Active Anticorrosive Coatings for Aluminum Alloys Part II: Influence of Nanocontainer Position

Dimitriya Borisova,^{*,†} Helmuth Möhwald,[†] and Dmitry G. Shchukin^{†,‡}

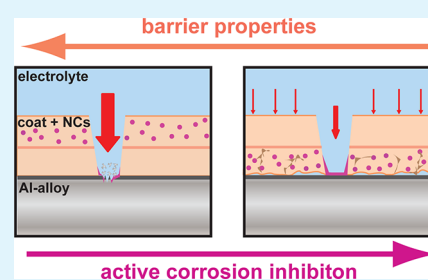
[†]Max Planck Institute of Colloids and Interfaces, Am Mühlenberg 1, 14424 Potsdam-Golm, Germany

[‡]Stephenson Institute for Renewable Energy, Department of Chemistry, The University of Liverpool, L69 4ZF Liverpool, United Kingdom

S Supporting Information

ABSTRACT: The present work contributes to the coating design of active anticorrosive coatings for the aluminum alloy, AA2024-T3. Part II is a continuation of Part I: Influence of Nanocontainer Concentration and describes further surprising aspects of the design of nanocontainer based active anticorrosive coatings, which influence their performance. The studied coating system consists of a passive sol-gel ($\text{SiO}_x/\text{ZrO}_x$) matrix and inhibitor (2-mercaptobenzothiazole) loaded mesoporous silica nanocontainers (MBT@NCs), which are dispersed only in half of the coating volume. Varying position and concentration of MBT@NCs the synergetic effect of inhibitor amount and path length on the metal surface were analyzed, considering the balance between optimum barrier properties, active protection and adhesion. The impact of MBT@NC position on passive and active corrosion resistance was investigated by electrochemical impedance spectroscopy and scanning vibrating electrode technique. Increasing the distance between MBT@NCs and metal surface led to better barrier properties but worse active corrosion inhibition. These findings improve the understanding of the factors influencing the overall performance of active anticorrosive coatings and enable the development of a coating system with optimum anticorrosion efficiency.

KEYWORDS: silica, nanocontainer, corrosion inhibitor, sol-gel, self-healing, aluminum alloy



INTRODUCTION

Metal destruction by corrosion leads to large maintenance costs in many industries.¹ The protection of metals from corrosion is a challenging task for materials science in view of increasing environmental requirements. For example, the development of nonchromated, “green alternatives” of potentially carcinogenic chromate conversion coatings for aluminum alloys used in aerospace industry has caused large research activity.^{2,3} The search for replacements has led to a new generation of self-healing coatings providing both passive and active protection.⁴ Passive protection is realized by intact coatings that function only as a physical barrier between the metal and the corrosive environment. In contrast, active protection offers corrosion inhibition when the coating is disrupted and the barrier properties are lost. One strategy to actively protect metals from corrosion is by the direct addition of corrosion inhibitors to coatings. However, this approach has several drawbacks such as degradation of coating integrity, inhibitor deactivation, or undesired leaching.^{5,6}

One way to avoid these disadvantages is the encapsulation of the corrosion inhibitors in nanocontainers (NCs) dispersed in the coating. The embedded NCs store the inhibitor and prevent any detrimental interaction with the coating matrix, thus improving its physical barrier properties. There are reports on different encapsulation approaches using nanotubes,⁷ porous

inorganic NCs,⁸ layered double hydroxides,⁹ polymer containers,¹⁰ and NCs with polyelectrolyte shells.¹¹ In all cases, the NCs are first loaded with the active agent and then randomly dispersed in the whole coating matrix without aiming at specific positioning within the coating. The inhibitor is released when the barrier properties of the coating are lost, i.e., at coating rupture. This release is triggered by changes in the local environment in the damaged area, such as changes in the local pH, ionic strength, humidity, or presence of aggressive ions.¹² The inhibitor molecules either deactivate the corrosive species or form a thin protective film over the exposed metal surface.^{13,14} Thus the anticorrosive properties of the coating are recovered because of the active protection offered by the encapsulated inhibitor.

Sol-gel thin coatings function as a pretreatment providing good adhesion to both metal surface and organic top coat.^{15,16} The elevated anticorrosion efficiency of sol-gel coatings incorporating inhibitor loaded metal oxide NCs has been already shown in several works of our group.^{17,18} However, the important effect of the embedded nanocontainer arrangement

Received: September 27, 2012

Accepted: December 13, 2012

Published: December 13, 2012

(e.g., nanocontainer concentration or position) on the overall performance of the coating has been described scarcely.

Previously, we demonstrated that the nanocontainer concentration in the coating matrix is a critical factor for achieving optimum anticorrosion efficiency.¹⁹ It was also suggested that the amount of available inhibitor should be sufficiently high for active protection and, at the same time, low enough to preserve good barrier properties of the coating. However, the distance between the inhibitor-loaded NCs and the metal surface to be protected is another important factor with a strong impact on the overall anticorrosion performance of the coating, which has not been studied so far. One might argue that active protection requires the NC to be as close to the Al surface as possible, but this in turn may affect barrier properties and adhesion. Therefore, these properties have to be studied separately to achieve optimally designed corrosion protection coatings based on nanocontainers. This study is the objective of the present work.

The studied coating systems consist of two layers of sol–gel ($\text{SiO}_x/\text{ZrO}_x$) coating dip-coated on the aluminum alloy, AA2024-T3. Two different coating systems were constructed in which the position and concentration of the 2-mercaptobenzothiazole (MBT) loaded mesoporous silica NCs (MBT@NCs) were varied (A: MBT@NCs in top layer and B: MBT@NCs in bottom layer). The physical and anticorrosive properties of the coating systems were studied in order to evaluate the effect of the distance between NCs (i.e., available inhibitor) and metal surface on the overall coating performance.

RESULTS AND DISCUSSION

Nanocontainers. In our previous work, we described the synthesis and properties of the mesoporous silica NCs used as inhibitor carriers in this report.¹⁸ Briefly, the spherical NCs are characterized by diameters in the range of 80 nm and high monodispersity ($\text{Pdl} \approx 0.07$) (see Figure S1a in the Supporting Information). The NC porosity is characterized by cylindrical open pores (diameter ~ 4 nm), oriented from the center to the outer surface of the NCs (see Figure S1b in the Supporting Information). The measured high surface area ($\sim 1000 \text{ m}^2 \text{ g}^{-1}$) and pore volume ($\sim 1 \text{ mL g}^{-1}$) are favorable for the adsorption of guest molecules. The adsorption of the inhibitor, 2-mercaptobenzothiazole (MBT), at the NCs was described in detail in ref 19. A high MBT loading (20 wt %) was achieved, which was found to be advantageous for active corrosion resistance.

Physical Properties of the Coatings. In this work, aluminum alloy AA2024-T3 was dip-coated with a hybrid inorganic sol–gel ($\text{SiO}_x/\text{ZrO}_x$) doped with MBT@NCs to form double-layer coating systems. Two coating systems differing in the position and concentration of the embedded MBT@NCs were designed: (A) double layer coating with the top layer doped with MBT@NCs and (B) double layer coating with the bottom layer doped with MBT@NCs. Different amounts of MBT@NCs were successfully dispersed in the sol–gel solution to obtain the following concentrations per one layer of the final cured double layer coating systems: 0, 0.04, 0.1, 0.2, 0.5, 0.7, 0.8, and 1.7 wt %. The thickness of the cured coatings deposited on the aluminum alloy was measured with a coating thickness gauge using the Eddy-current principle.²⁰ Similar coating thicknesses in the range of 4–5 μm were obtained for both coating systems (Figure 1). Considering the measurement error ($\sim 30\%$) due to the high metal surface roughness and thin coatings, the measured thicknesses of the

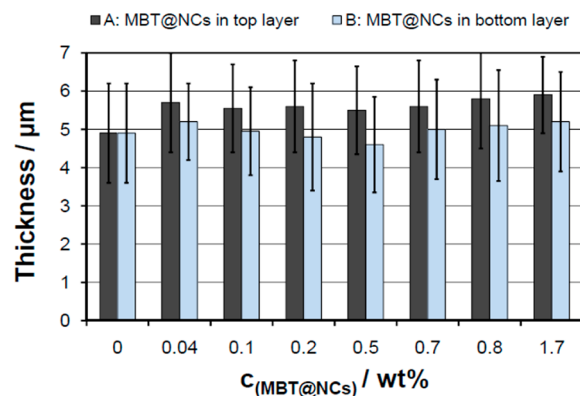


Figure 1. Measured coating thicknesses of the cured double layer coatings containing different concentrations of MBT@NCs in the (A) top or (B) bottom layer.

double layer coatings are comparable with the ones of the single layer coatings (4–5 μm) described in our previous work.¹⁹ Taking this into account as well as the coating design, we can assume that the concentration of MBT@NCs in the volume of the whole double-layer coating systems is around two times lower compared to the single-layer coating system.

Using a pull-off test according to the standard method, ASTM D4541, the dry adhesion of the freshly cured coatings was determined. The pull-off force needed for detachment of an aluminum pull-stub glued to the coated sample is divided by the test area to express adhesion as tensile stress. The measured adhesion values of both coating systems to the metal surface are comparable and in the range of 2–3 MPa (Figure 2).^{21–23}

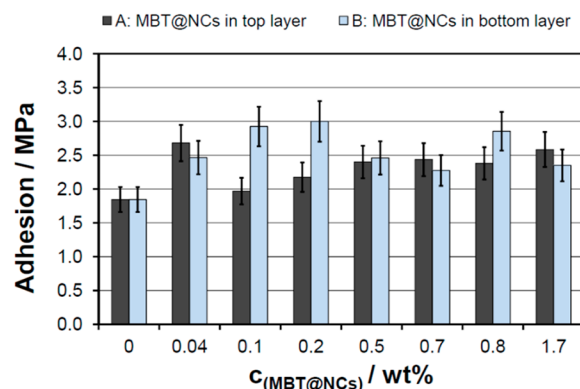


Figure 2. Measured adhesion of the freshly cured double-layer coatings with MBT@NCs in the (A) top or (B) bottom layer to the metal substrate (AA2024-T3).

Coating adhesion did not correlate with embedded MBT@NC concentration in a defined way. However, coatings with MBT@NCs demonstrate comparable or slightly higher adhesion to the metal than the ones without MBT@NCs. This suggests that embedding MBT@NCs in the sol–gel matrix improves the stability of the coating and its adhesion to the metal. Furthermore, a complete removal of both coating layers was observed for all samples. This is an indication for good adhesion between the two layers of the double-layer coating system.

Anticorrosive Properties of the Coatings. *Active Corrosion Resistance.* To evaluate the active corrosion resistance of the coated samples, the evolution of corrosion

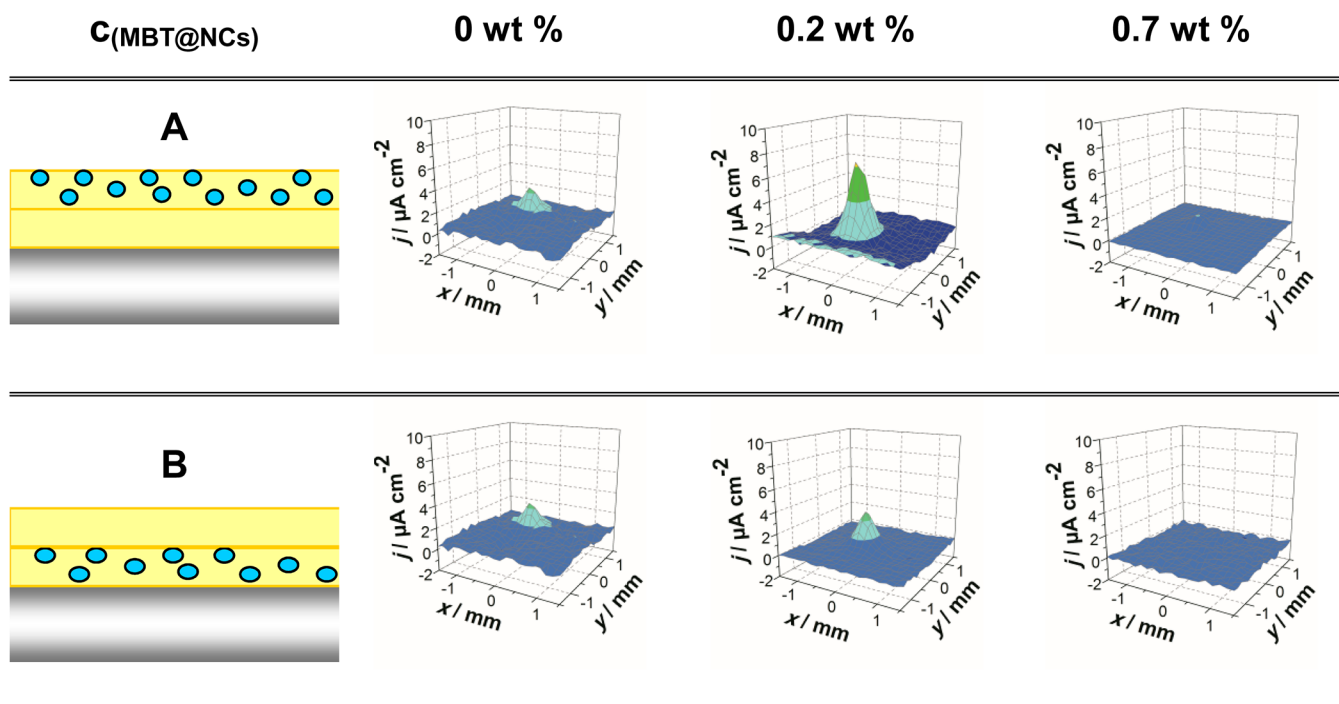


Figure 3. SVET 3D current density maps of the studied coating systems A and B (left). Examples of coated samples with detected high (MBT@NCs = 0.2 wt %) and low (MBT@NCs = 0.7 wt %) anodic current densities in comparison to the control (MBT@NCs = 0 wt %) after 12 h immersion in 0.1 M NaCl.

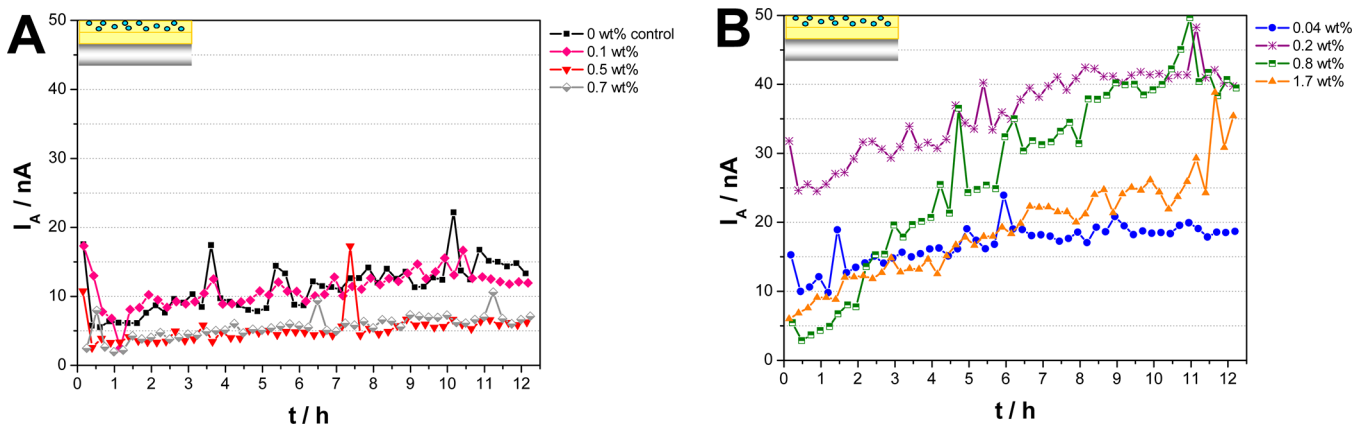


Figure 4. Maximum anodic currents detected with SVET over the scanned scratched area during a 12 h immersion period in 0.1 M NaCl. Results are shown for samples coated with two layers of sol–gel containing different MBT@NC concentrations in the top layer demonstrating (a) efficient and (b) unsatisfactory active corrosion inhibition.

in an artificial scratch in the coating was studied using the scanning vibrating electrode technique (SVET). The galvanic coupling between the intermetallic particles and the surrounding aluminum matrix in the aluminum alloy, AA2024-T3, used as a substrate, promotes localized, pitting corrosion. Upon initiation of corrosion the electrochemical reactions occurring at the metal surface cause a positive anodic and a negative cathodic ionic current flow, which leads to potential differences in the electrolyte solution. Employing SVET, these potential differences are measured and converted into an electrical current density over the scanned area. For the quantification of the overall electrochemical activity, the current density maps taken periodically were integrated to calculate the minimum (cathodic) and maximum (anodic) currents as a function of time.^{24,25} The 3D current density maps obtained for exemplary coated samples after 12 h immersion are depicted in Figure 3.

The anodic activity is represented as a single positive peak with a constant position indicating the site of a corrosion anode. The anodic peak intensity is proportional to the degree of metal dissolution. In contrast, a cathodic activity related to the oxygen reduction is poorly pronounced and not characterized by a localized peak. Therefore, the hardly detected cathodic current that is not a direct measure of aluminum degradation is not plotted as a function of time.²⁶ Instead, the efficiency of corrosion inhibition is described by the increase of the anodic current (Figures 4 and 5). Coated samples exhibiting higher anodic activity than the control sample without inhibitor possess no self-healing properties. If the MBT@NCs are embedded in the top layer of the coating (coating system A), most of the studied samples fail to actively inhibit corrosion (Figure 4). The samples with too low MBT@NC concentration (0.04–0.2 wt %) provide insufficient amount of

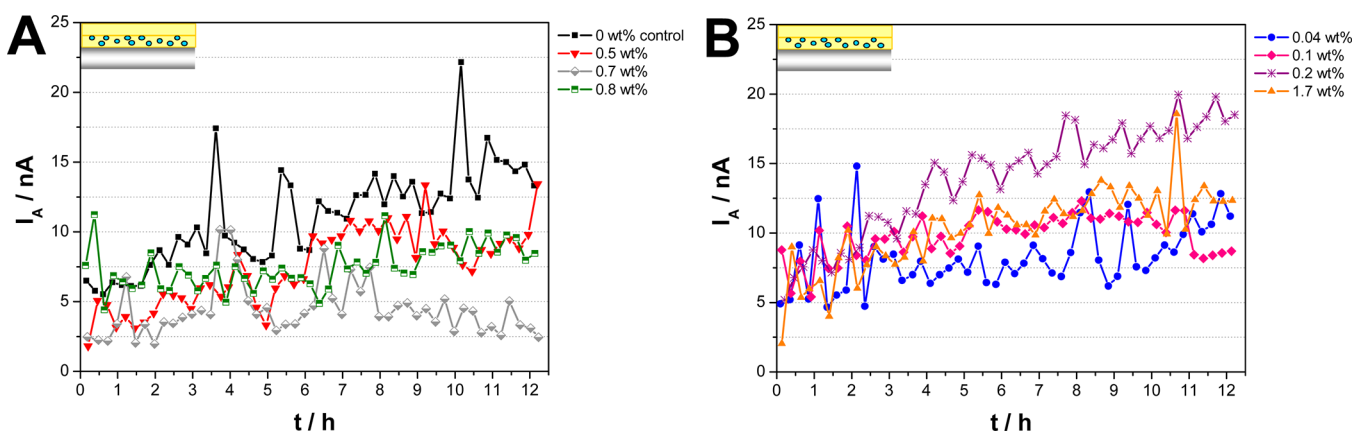


Figure 5. Maximum anodic currents detected with SVET over the scanned scratched area during a 12 h immersion period in 0.1 M NaCl. Results are shown for samples coated with two layers of sol–gel containing different MBT@NC concentrations in the bottom layer exhibiting a) efficient and b) unsatisfactory active corrosion inhibition. Note that the plotted I_A is for a smaller anodic current range than in Figure 4.

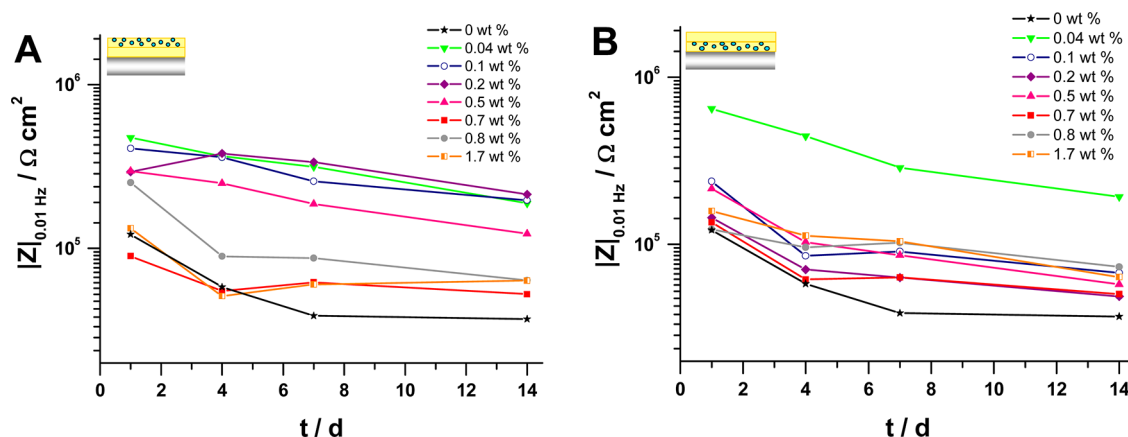


Figure 6. $|Z|$ values measured at the lowest frequency, 0.01 Hz (plotted on a logarithmic scale) over the course of the EIS study in 1 M NaCl. Results for the intact, double layer coating systems containing different MBT@NC concentrations in (a) the top or (b) the bottom layer are shown.

corrosion inhibitor to stop the corrosion propagation, which results in higher anodic activity than the control. Surprisingly, very high amount of available inhibitor (i.e., higher $c(\text{MBT@NCs}) = 0.8\text{--}1.7\text{ wt \%}$) in the coating system A does not favor the corrosion inhibition. These results can be explained by a possible deterioration of the coating matrix at the areas neighboring the scratch. This is due to the high amount of embedded NCs leading to more paths for the aggressive chloride ions and larger area for corrosive attack. As a result, the amount of available inhibitor at these larger corrosion attack sites is not enough to inhibit the undergoing corrosion. Thus, the samples in which the top layer contains MBT@NCs of intermediate concentrations (0.5–0.7 wt %) provide the best corrosion inhibition and suppress the anodic current at around 5 nA in comparison to the lower and higher NC concentrations.

In contrast, the samples with MBT@NCs in the bottom layer (coating system B) close to the metal surface show lower anodic activity (maximum $I_A \sim 20\text{ nA}$) than the samples with MBT@NCs in the top layer, qualifying them as coating systems providing better active protection (Figure 5). A possible explanation could be the shorter distance between the MBT@NCs and the attacked metal surface providing a shorter diffusion length and time for the inhibitor molecules to reach the corrosion initiation site and to form a surface complex to inhibit corrosion propagation. Furthermore, in the coating

system B, no well-pronounced differences in the detected anodic currents for too high or too low MBT@NC concentrations were observed. However, the anodic current measured for the sample with 0.7 wt % MBT@NCs in the bottom layer was an exception to this trend and remained at the lowest level of 5 nA. Based on the SVET results, the optimum MBT concentration loaded into nanocontainers and needed for sufficient active corrosion inhibition was determined to be 0.14 wt % (corresponds to $c(\text{MBT@NCs}) = 0.7\text{ wt \%}$) for both double layer coating systems. In addition, the double layer coating systems suppressed the anodic activity better than the single layer coatings described previously (see Figure S2 in the Supporting Information).¹⁹ The corrosion propagation in samples coated with a single sol–gel led to anodic currents above 50 nA. This finding suggests that introducing a second layer in the coating improves the active anticorrosive properties.

Passive Corrosion Resistance. The barrier properties and passive corrosion resistance of the double layer coatings were studied with electrochemical impedance spectroscopy (EIS). The coated AA2024-T3 plates were exposed to 1 M NaCl for 14 days and EIS spectra were collected at different time intervals. The change of anticorrosion performance of the studied coating systems with time was evaluated by comparing the impedance modulus at the lowest measured frequency ($|Z|_{0.01\text{ Hz}}$), which reflects the corrosion resistance (Figure 6). The relative impedance decrease for all coatings containing

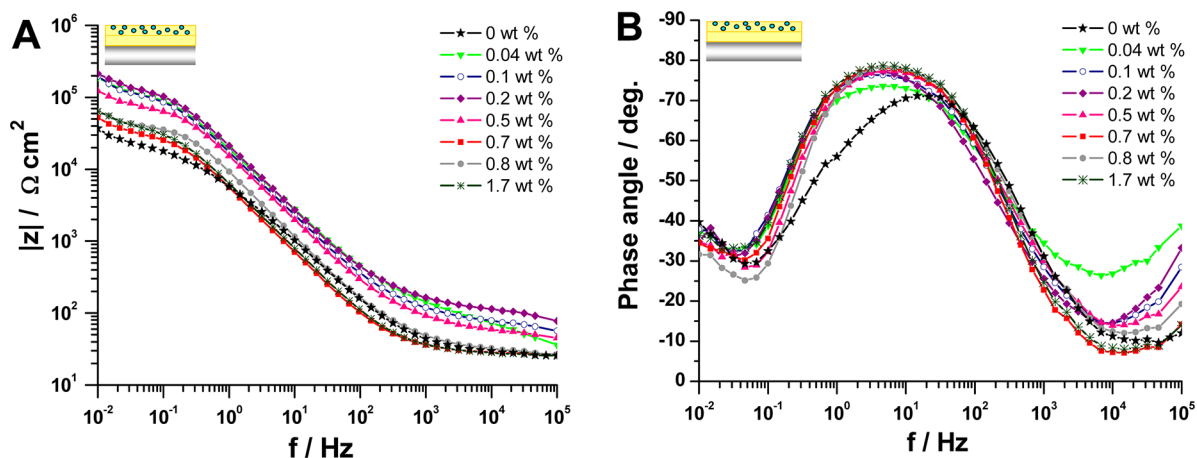


Figure 7. EIS data obtained after 14 days immersion in 1 M NaCl and represented as a Bode plot showing the change in (a) absolute impedance and (b) phase angle as a function of frequency for double-layer coatings containing different MBT@NC concentrations in the top layer.

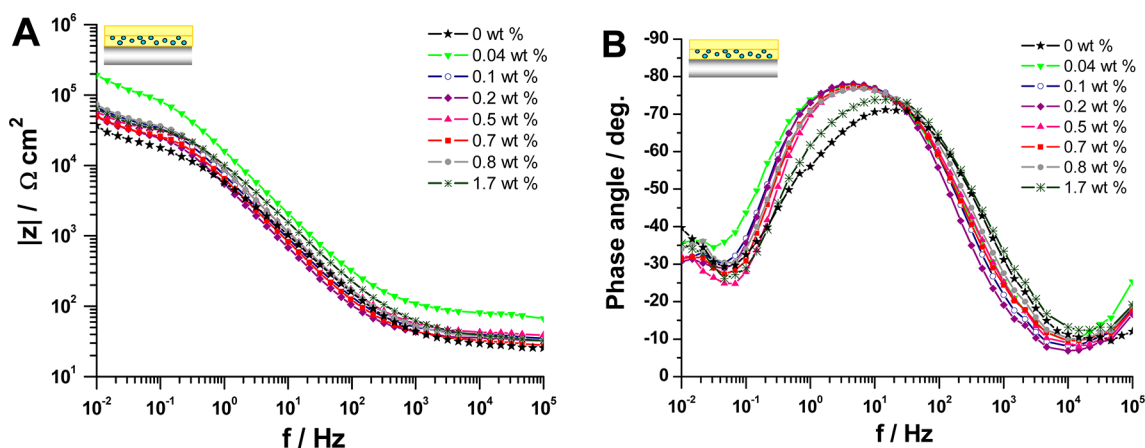


Figure 8. EIS data obtained after 14 days immersion in 1 M NaCl and represented as a Bode plot showing the change in (a) absolute impedance and (b) phase angle as a function of frequency for double layer coatings containing different MBT@NC concentrations in the bottom layer.

MBT@NCs is comparable, which suggests a comparable degradation rate. However, for low MBT@NC concentrations ($c < 0.7$ wt %), the coating system with MBT@NCs in the top layer exhibits higher absolute impedance values over the whole course of the test compared to the coating system with MBT@NCs in the bottom layer. These results suggest that introducing MBT@NCs in the top layer at concentrations higher than 0.5 wt % leads to a deterioration of the coating barrier properties (Figure 6a). This detrimental effect is observed at even lower concentrations with a threshold of 0.04 wt % when the MBT@NCs are embedded in the bottom layer (Figure 6b). Nevertheless, the comparison of the normalized $|Z|_{0.01 \text{ Hz}}$ values for single and double layer coatings demonstrates the superior barrier properties of the double layer coatings (see Figure S3 in the Supporting Information). This can be attributed only to the coating design because the coating thickness of all coatings is similar. The optical photographs of the coated samples after 14 days immersion in 1 M NaCl reveal some black pits and white deposits, which indicate corrosion attack (see Figure S4 in the Supporting Information). The visual observation is reflected in the EIS spectra (Figures 7 and 8), which can be characterized by three time constants. The high frequency time constant (1×10^5 Hz) can be ascribed to the coating response (CPE_{coat} and R_{coat}). The second time constant at intermediate frequencies is usually associated with the native aluminum oxide layer.

However, after 14 days immersion of the studied coatings, the oxide layer was deteriorated and could not be detected because of the ongoing corrosion as inspected visually. Therefore, the occurrence of corrosion (CPE_{di} and R_{ct}) dominated the EIS spectra after 14 days and was described by the second time constant (1–10 Hz). The third time constant at the lowest frequency (0.01 Hz) describes the mass transport of corrosion products and corrosive agents between metal surface and electrolyte.^{27–29} An equivalent circuit including the above-mentioned time constants is shown in Figure 9c and was used to numerically fit the EIS spectra for both double layer coatings obtained after 14 days immersion in 1 M NaCl (Figures 7 and 8). This fitting model was chosen because it describes very well the electrochemical response of the relaxation processes occurring in the coated samples and delivers a good fit quality ($\chi^2 \approx 0.01$).

Constant phase elements (CPE) instead of capacitances were used for the fitting because the phase angles deviated from -90° . The values for capacitance were calculated using the following equation

$$C = Q(\omega_{\text{max}})^{n-1} \quad (1)$$

in which ω_{max} is the radial frequency at which Z'' reaches a maximum for the respective time constant, Q and $0 < n \leq 1$ are parameters calculated for the CPE by fitting.³⁰

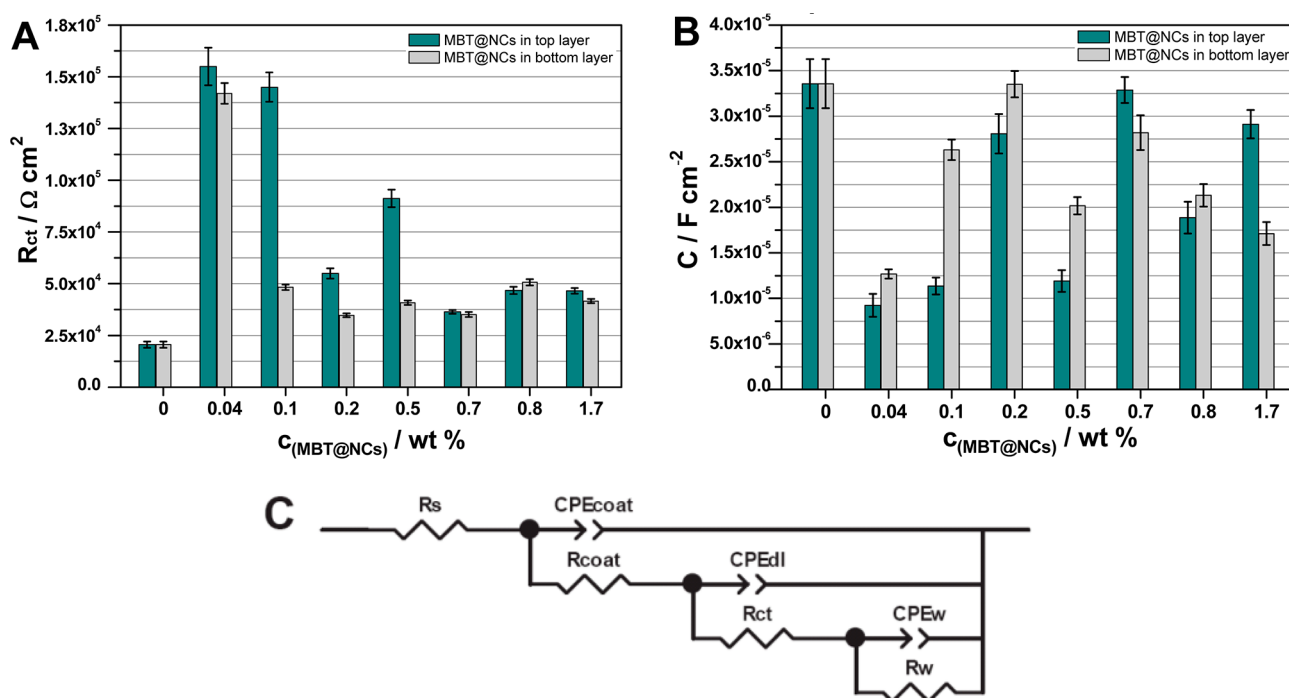


Figure 9. Calculated data for (a) the charge transfer resistance (R_{ct}) and (b) double layer capacitance (C_{dl}) obtained by fitting of the EIS spectra using (c) the equivalent circuit. EIS spectra of both double-layer coating systems measured after 14 days immersion in 1 M NaCl were fitted.

The calculated values for the charge transfer resistance (R_{ct}) and double layer capacitance (C_{dl}) are presented because these parameters directly indicate the extent of corrosion (Figure 9a, b). Good coating barrier properties are revealed by high R_{ct} and low C_{dl} values. The R_{ct} values for all coatings containing MBT@NCs are higher than for the bare coating. This can be due to the embedded inhibitor, which inhibits the corrosion attack and increases R_{ct} . The incorporation of MBT@NCs at concentrations above 0.5 wt % leads to a comparable electrochemical response for both coating designs. The integration of high MBT@NC concentrations can lead to a degradation of the coating and additional diffusion paths around possible MBT@NC agglomerates. These detrimental effects explain the worse passive corrosion resistance of both coating systems containing high amount of MBT@NCs ($c > 0.5$ wt %). However, if a small amount of MBT@NCs is embedded, more pronounced differences between the two coating systems can be observed. If the layer with the MBT@NCs is separated from the metal by a bare sol-gel layer, the coating system reveals superior passive corrosion resistance. This can be due to a better adhesion to the aluminum surface of a bare sol-gel layer than a sol-gel layer with MBT@NCs. Thus, the barrier properties of double layer coatings with low MBT@NC concentrations in the top layer compared to the ones with MBT@NCs in the bottom layer are better due to a preserved coating integrity and good adhesion between coating and metal surface. However, the incorporation of more MBT@NCs leads to the loss of this effect and to a comparable passive corrosion resistance of both coating designs. On the other hand, the addition of NCs to the bottom layer provides better self-healing ability to the coating.

CONCLUSIONS

This work presents a new design of active anticorrosive coatings for the aluminum alloy, AA2024-T3. It contributes to the study of the effects influencing the efficiency of active

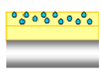
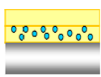
anticorrosive coatings with embedded nanocontainers. The model coating system used for this investigation is based on a passive sol-gel matrix in which MBT-loaded mesoporous silica nanocontainers (MBT@NCs) are embedded. In Part I (Influence of nanocontainer concentration) of this work,¹⁹ it was found that a compromise between delivering an optimal amount of corrosion inhibitor and preserving the coating barrier properties is required in order to attain satisfactory anticorrosion performance. In Part II, the MBT@NC position in the coating, as another import factor influencing anticorrosion efficiency, is investigated. Introducing the MBT@NCs close to the metal surface facilitates the fast transport of released inhibitor upon corrosion attack and improves the active corrosion resistance and self-healing ability. On the other hand, better barrier properties are observed for double-layer coatings with MBT@NCs in the top layer because of a preserved coating integrity and good adhesion between coating and metal surface. On the basis of this study, optimum active and passive corrosion resistance are provided by double-layer coatings containing intermediate MBT@NC concentrations (0.5–0.7 wt %) in the top layer.

Although the results obtained in this study describe a specific system, they also provide general information about the factors influencing the anticorrosion performance and properties of active anticorrosive coatings with embedded nanocontainers.

EXPERIMENTAL SECTION

Materials. Tetraethyl orthosilicate (TEOS, $\geq 99\%$), triethanolamine (TEA), hexadecyl trimethyl-ammoniumchloride (CTACl, 25% in H_2O) and (3-glycidioxypropyl) trimethoxysilane (GPTMOS, $\geq 98\%$) were purchased from Sigma-Aldrich and used without further purification. Zirconium(IV) propoxide solution (TPOZ, 70 wt % in 1-propanol) and ethyl acetoacetate (EAA) were supplied by Alfa Aesar and used as received. Hydrochloric acid (HCl, 37%) and nitric acid (HNO_3 , 65%) were purchased from Carl Roth. Sodium hydroxide (NaOH, 1 M), sodium chloride (NaCl, analytical grade) and 2-

Chart 1. Summary of the Tested Coating Systems

Coating label	Coating design	Description	c(MBT@NCs) in cured coating [wt %]
A		two layers, MBT@NCs in top layer	0.04; 0.1; 0.2; 0.5; 0.7; 0.8; 1.7
B		two layers, MBT@NCs in bottom layer	0.04; 0.1; 0.2; 0.5; 0.7; 0.8; 1.7

mercaptobenzothiazole (MBT) were provided by Merck. Ethanol (EtOH) and propan-2-ol (IPA) were obtained from VWR Prolabo. The Milli-Q water used in all experiments was distilled in a three-stage Millipore Milli-Q Plus 185 purification system. The aluminum alloy, AA2024-T3, used for corrosion testing was provided by EADS Deutschland. A two-component adhesive (3M, Scotch-Weld DP 490) was used for adhesion tests.

Synthesis Methods. Mesoporous silica NCs were prepared as described in our previous work.¹⁸ The synthesized NCs were subsequently loaded with a corrosion inhibitor (MBT). An ethanol solution of MBT (20 mg mL⁻¹) was added to a silica-ethanol suspension (20 mg mL⁻¹) in 1:1 volume ratio and stirred for 4 h under reduced pressure (50 mbar). Subsequently, the mixture was centrifuged to obtain the loaded NCs (MBT@NCs), which were then dried overnight at 60 °C.

The hybrid SiO_x/ZrO_x sol was prepared using a sol-gel process, as reported previously³¹ and used for the subsequent dip-coating of the aluminum alloy (AA2024-T3) substrates. The aluminum substrates were pretreated first in 1 M NaOH for 15 min at 60 °C, then in 20 wt % HNO₃ for 15 min at room temperature and finally washed with Milli-Q water and dried with N₂ flow. The cleaned substrates were dipped in the respective sol-gel mixture for 100 s and then pulled out at a speed of 2 mm s⁻¹ (Bungard RDC 15 dip coater). The coated samples were cured at 130 °C for 1 h after each dipping. The second layer was deposited on the cured layer in order to ensure the dispersion of the nanocontainers only in one layer.

Following this dipping procedure, different coating systems consisting of two layers were produced. These differed in the position and concentration of MBT@NCs dispersed in the coating layers. The design of the coating systems can be divided into: (A) double-layer coatings with the top layer doped with MBT@NCs and (B) double layer coatings with the bottom layer doped with MBT@NCs. The MBT@NC concentration was varied in both coating systems and was calculated to be 0.04, 0.1, 0.2, 0.5, 0.7, 0.8, and 1.7 wt % in the final cured coating layer containing the MBT@NCs.

Characterization Methods. The silica NCs and the coated metal samples were investigated with scanning electron microscopy (Zeiss Gemini LEO 1550). Transmission electron microscopy (Zeiss EM 912 Omega) with an accelerating voltage of 120 kV was used to characterize the morphology, size and pore structure of the synthesized NCs.

A coating thickness gauge, Surfex Pro S, from PHYNIX, Germany, using the Eddy-current principle was used to measure the coating thickness. A coating thickness probe, FN1.5, attached to a stand and used in a nonferrous (FN) measuring mode detected the changes in the current flows induced by different coating thicknesses.

An adhesion tester PosiTest AT-A, DeFelsko was used to measure the adhesion of freshly cured coatings to the metal substrate, following the standard adhesion test method, ASTM D4541. Aluminum pull-stubs glued to the freshly cured coated samples were detached to remove the coating from the substrate and measure the adhesion of coating to metal substrate. The pull-off force needed for detachment was divided by the test area to obtain adhesion as tensile stress.

The scanning vibrating electrode technique (SVET, Applicable Electronics) was used to investigate the active anticorrosive properties of the coated samples in 0.1 M NaCl solution. In order to expose the metal to the 0.1 M NaCl solution, an artificial defect was introduced into the coating prior to immersion. Using a scalpel blade (Bayha blade No. 22) attached to a lever, a controlled, straight scratch was made in the coating with the following dimensions: width ~20 μm, length ~2 mm and depth ~60 μm. The sample was then sealed and only the area (3 × 3 mm²) containing the scratch was exposed to the 0.1 M NaCl solution for 12 h. A vibrating Pt-blackened electrode tip with a diameter of 20 μm scanned the exposed coated sample area every 15 min at 300 μm above the surface. The electrode vibrated with a frequency of 864 Hz and amplitude of 40 μm and recorded the vertical current density.

For electrochemical impedance spectroscopy (EIS) an area of 3 cm² of the coated substrates (6 × 3 cm²) was exposed to 1 M NaCl solution. Impedance spectra were recorded using a three-electrode setup consisting of a reference (saturated calomel), a counter (platinum) electrode and a working electrode (metal substrate). A CompactStat electrochemical analyzer (Ivium Technologies) was used to perform the measurements in a Faraday cage. A frequency range of 0.01 Hz to 1 MHz at a constant potential (1 V) was used to obtain the current response of the coated sample with Ivium Soft (release 1.985) software. The spectra were obtained using six frequencies per decade and a sinusoidal voltage signal of 10 mV amplitude. The subsequent fitting of the results was done with Zview software and the spectra were normalized with the area of the working electrode (3 cm²) in order to obtain impedance in Ω cm².

■ ASSOCIATED CONTENT

📄 Supporting Information

Additional characterization data of single layer coatings and nanocontainers, photographs after EIS test and Nyquist plots for the double layer coating systems. This material is available free of charge via the Internet at <http://pubs.acs.org>

■ AUTHOR INFORMATION

Corresponding Author

*E-mail: borisova@mpikg.mpg.de.

Notes

The authors declare no competing financial interest.

■ ACKNOWLEDGMENTS

We thank M. Schenderlein for TGA measurements, R. Rothe for BET analysis, J. Tedim and K. Yasakau (CICECO, University of Aveiro, Portugal) for help with EIS data fitting. This work was financially supported by the ForMat program of the German Ministry for Science and Education (BMBF) and a German-Portuguese DAAD project.

■ REFERENCES

- (1) Schmitt, G.; Schütze, M.; Hays, G. F.; Burns, W.; Han, E.-H.; Pourbaix, A.; Jacobson, G. World Corrosion Organization: New York, 2009, 5–15.
- (2) EPA Federal Register; U.S. Environmental Protection Agency: Washington, D.C., 1995; Vol. 60, p 45947.
- (3) Twite, R. L.; Bierwagen, G. P. *Prog. Org. Coat.* **1998**, *33*, 91–100.
- (4) Hughes, A. E.; Cole, I. S.; Muster, T. H.; Varley, R. J. *NPG Asia Mater.* **2010**, *2*, 143–151.
- (5) Garcia-Heras, M.; Jimenez-Morales, A.; Casal, B.; Galvan, J. C.; Radzki, S.; Villegas, M. A. *J. Alloys Compd.* **2004**, *380*, 219–224.
- (6) Voevodin, N. N.; Grebasch, N. T.; Soto, W. S.; Arnold, F. E.; Donley, M. S. *Surf. Coat. Technol.* **2001**, *140*, 24–28.
- (7) Lvov, Y. M.; Shchukin, D. G.; Möhwald, H.; Price, R. R. *ACS Nano* **2008**, *2*, 814–820.
- (8) Pomorska, A.; Yliniemi, K.; Wilson, B. P.; Shchukin, D.; Johannsmann, D.; Grundmeier, G. *J. Colloid Interface Sci.* **2011**, *362*, 180–187.
- (9) Wang, Y.; Zhang, D. *Mater. Res. Bull.* **2011**, *46*, 1963–1968.
- (10) Latnikova, A.; Grigoriev, D. O.; Hartmann, J.; Möhwald, H.; Shchukin, D. G. *Soft Matter* **2011**, *7*, 369–372.
- (11) Shchukin, D. G.; Möhwald, H. *Small* **2007**, *3*, 926–943.
- (12) Samadzadeh, M.; Boura, S. H.; Peikari, M.; Kasirih, S. M.; Ashrafi, A. *Prog. Org. Coat.* **2010**, *68*, 159–164.
- (13) Harvey, T. G.; Hardin, S. G.; Hughes, A. E.; Muster, T. H.; White, P. A.; Markley, T. A.; Corrigan, P. A.; Mardel, J.; Garcia, S. J.; Mol, J. M. C.; Glenn, A. M. *Corros. Sci.* **2011**, *53*, 2184–2190.
- (14) Lamaka, S. V.; Zheludkevich, M. L.; Yasakau, K. A.; Montemor, M. F.; Ferreira, M. G. S. *Electrochim. Acta* **2007**, *52*, 7231–7247.
- (15) Guglielmi, M. J. *Sol–Gel Sci. Technol.* **1997**, *8*, 443–449.
- (16) van Ooij, W. J.; Zhu, D. Q.; Prasad, G.; Jayaseelan, S.; Fu, Y.; Teredesai, N. *Surf. Eng.* **2000**, *16*, 386–396.
- (17) Hollamby, M. J.; Borisova, D.; Möhwald, H.; Shchukin, D. *Chem. Commun.* **2012**, *48*, 115–117.
- (18) Borisova, D.; Möhwald, H.; Shchukin, D. G. *ACS Nano* **2011**, *5*, 1939–1946.
- (19) Borisova, D.; Möhwald, H.; Shchukin, D. G. *ACS Appl. Mater. Interfaces* **2012**, *4*, 2931–2939.
- (20) Kral, J.; Smid, R.; Ramos, H. M. G.; Ribeiro, A. L. In *2011 IEEE Instrumentation and Measurement Technology Conference (I2MTC)*; IEEE: Piscataway, NJ, 2011; pp 1–6.
- (21) Rickerby, D. S. *Surf. Coat. Technol.* **1988**, *36*, 541–557.
- (22) Mohler, J. B. *Met. Finish.* **1983**, *81*, 71–73.
- (23) ASTM Standard D4541: Standard Test Method for Pull-Off Strength of Coatings Using Portable Adhesion Testers; ASTM International: West Conshohocken, PA, 2009; DOI: 10.1520/D4541-09E01, .
- (24) He, J.; Gelling, V. J.; Tallman, D. E.; Bierwagen, G. P. *J. Electrochem. Soc.* **2000**, *147*, 3661–3666.
- (25) Lamaka, S. V.; Taryba, M.; Montemor, M. F.; Isaacs, H. S.; Ferreira, M. G. S. *Electrochim. Commun.* **2011**, *13*, 20–23.
- (26) Fix, D.; Skorb, E. V.; Shchukin, D. G.; Möhwald, H. *Meas. Sci. Technol.* **2011**, *22*.
- (27) Zheludkevich, M. L.; Serra, R.; Montemor, M. F.; Yasakau, K. A.; Salvado, I. M. M.; Ferreira, M. G. S. *Electrochim. Acta* **2005**, *51*, 208–217.
- (28) Matter, E. A.; Kozhukharov, S.; Machkova, M.; Kozhukharov, V. *Corros. Sci.* **2012**, *62*, 22–33.
- (29) Maia, F.; Tedim, J.; Lisenkov, A. D.; Salak, A. N.; Zheludkevich, M. L.; Ferreira, M. G. S. *Nanoscale* **2012**, *4*, 1287–1298.
- (30) Hsu, C. H.; Mansfeld, F. *Corrosion* **2001**, *57*, 747–748.
- (31) Zheludkevich, M. L.; Serra, R.; Montemor, M. F.; Salvado, I. M. M.; Ferreira, M. G. S. *Surf. Coat. Technol.* **2006**, *200*, 3084–3094.